

Growth kinetics, structure, and morphology of para-quaterphenyl thin films on gold(111)

S. Müllegger,^{a)} I. Salzmann, and R. Resel

Institute of Solid State Physics, Graz University of Technology, Petersgasse 16, A-8010 Graz, Austria

G. Hlawacek and C. Teichert

Institute of Physics, University of Leoben, Franz Josef Strasse 18, A-8700 Leoben, Austria

A. Winkler

Institute of Solid State Physics, Graz University of Technology, Petersgasse 16, A-8010 Graz, Austria

(Received 29 January 2004; accepted 7 May 2004)

The adsorption, desorption, and growth kinetics as well as the thin film morphology and crystal structure of *p*-quaterphenyl (4P) grown under ultrahigh vacuum conditions on single crystalline Au(111) have been investigated. Thermal desorption spectroscopy (TDS) reveals two distinct first-order peaks attributed to monolayer desorption followed by a zero-order multilayer desorption. The saturation coverage of the full 4P monolayer has been quantitatively measured with a quartz microbalance to be 8×10^{13} molecules/cm². Using low energy electron diffraction the structures of the 0.5 and 1 ML (monolayer) adsorbates have been studied, showing highly regular arrangements of the 4P molecules, which are affected by the (111) surface structure. At the transition from 0.5 to 1 ML a structural compression of the overlayer has been observed. The behavior of thicker 4P films has been investigated by combined TDS-XPS (XPS—x-ray photoelectron spectroscopy). A temperature-induced recrystallization process at about 270 K has been observed for a 7 nm thick 4P film grown at 93 K, corresponding to a transition from a disordered layerlike growth to a crystalline island growth. *Ex situ* optical microscopy and atomic-force microscopy investigations have revealed needle-shaped 4P islands. Applying x-ray diffraction the crystalline order and epitaxial relationship of the 4P films with 30 nm and 200 nm mean thicknesses have been determined. © 2004 American Institute of Physics. [DOI: 10.1063/1.1767154]

I. INTRODUCTION

Conjugated organic materials have become promising candidates for various applications in molecular electronics and optoelectronics.^{1–3} Amongst other materials oligophenylenes have been successfully used as active materials in organic light-emitting diodes^{4,5} or in organic thin film transistors.⁶ The fabrication of well-oriented highly crystalline thin films as well as the control of the organic/substrate interface are important not only for optimizing the device performance but also for exploring the underlying physics.^{7,8} Several studies have been carried out on oligophenylene thin films grown on various substrates concerning the crystal structure,^{9,10} thin film morphology,¹¹ and optical and electronic properties.^{12–14}

The focus of the present study was to investigate the adsorption/desorption kinetics, the structure, as well as the thin film morphology of our model system *p*-quaterphenyl (4P), grown on single crystalline Au(111) under well-defined conditions. The emphasis was placed on the application of surface-sensitive techniques to investigate the organic/substrate interface. A variety of analytical methods were applied such as thermal desorption spectroscopy (TDS), x-ray photoelectron spectroscopy (XPS), Auger electron spectroscopy (AES), x-ray diffraction (XRD), optical microscopy (OM), and atomic-force microscopy (AFM). In particular, the structure of the 4P overlayer in the submonolayer and monolayer regimes was investigated using low energy electron diffraction (LEED).

copy (AES), x-ray diffraction (XRD), optical microscopy (OM), and atomic-force microscopy (AFM). In particular, the structure of the 4P overlayer in the submonolayer and monolayer regimes was investigated using low energy electron diffraction (LEED).

II. EXPERIMENTAL METHODS

The sample preparation as well as the TDS, XPS, AES, and LEED measurements were performed *in situ* under ultrahigh vacuum conditions with a base pressure of $\sim 10^{-10}$ mbar. The substrate was a high-purity Au single crystal (MaTeCK GmbH) cut along the (111) plane with an angular deviation of less than 0.4°. It was cleaned by standard Ar⁺-ion sputtering (5×10^{-5} mbar, 1 kV) for 30 min and subsequent annealing at 870 K for 10 min. AES and XPS were used to check the purity of the Au surface. In this context it should be noted that some 4P dissociation was observed on the Au(111) surface upon heating of a 4P film, resulting in a remaining carbon coverage of about 0.03 monolayer (ML). Higher carbon coverages could intentionally be obtained by x-ray irradiation of a 4P film. The influence of a carbon precoverage on the kinetics and growth of 4P films on Au(111) will be treated in detail in a separate publication.¹⁵ For the present investigations the Au sample was thoroughly cleaned prior to each 4P film preparation step in order to ensure a minimum influence of surface carbon on

^{a)} Author to whom correspondence should be addressed; Electronic address: stefan.muellegger@tugraz.at

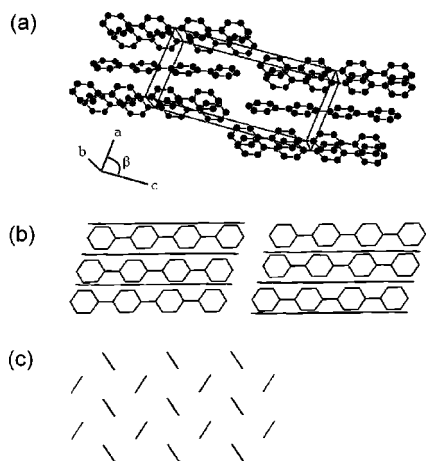


FIG. 1. Quaterphenyl crystal structure at room temperature. (a) The monoclinic 4P unit cell ($a=0.811$ nm, $b=0.561$ nm, $c=1.791$ nm, and $\beta=95.80^\circ$) contains two molecules that are tilted with respect to each other. (b) The 4P molecules form stacked layers that can be clearly seen by projecting the structure along the a axis of the unit cell. (c) The molecular arrangement within each layer is illustrated by a projection along the long molecular axes, revealing a herringbone structure.

the measurements. The 4P films were vacuum deposited from a home-made quartz glass Knudsen cell at a deposition rate of 0.24–0.72 nm/min. Details on the quantification of the TD spectra are described in Ref. 16.

The film structure at low 4P coverage (≤ 1 ML) was investigated with an OMICRON LEED instrument equipped with a single microchannelplate. The low emission current (nA) prevented the organic films from potential damage by electron bombardment. All LEED images were taken at 93 K in order to get an optimum signal-to-noise ratio. The XRD as well as OM and AFM measurements were performed *ex situ* at room temperature. The crystalline order and the epitaxial relationship of 30 nm and 200 nm thick 4P films were investigated with a Philips X'Pert texture goniometer with Cr $K\alpha$ radiation. For direct imaging of the surface morphology of 4P films on the nanometer scale atomic-force microscopy measurements were performed using a Digital Instruments MultiMode AFM under ambient conditions. The measurements were done in tapping mode at very low scan speeds to avoid destruction of the 4P film by the probe.

The crystal structure of solid quaterphenyl at 300 K is shown in Fig. 1(a). The monoclinic unit cell comprises two molecules and the symmetry is $P2_1/a$. The lattice constants are $a=0.811$ nm, $b=0.561$ nm, and $c=1.791$ nm, and the monoclinic angle is $\beta=95.80^\circ$.^{17,18} The 4P molecules form stacked layers which can be seen under a proper projection of the crystal structure as shown in Fig. 1(b). The molecular packing within each layer is of the typical herringbone type. This can be seen by projecting the crystal structure along the direction of the long molecular axes, which is illustrated in Fig. 1(c).

III. RESULTS AND DISCUSSION

A. Desorption kinetics

A series of TD spectra for 4P grown on Au(111) at 93 K is shown in Fig. 2. Starting from a low 4P coverage, the TDS

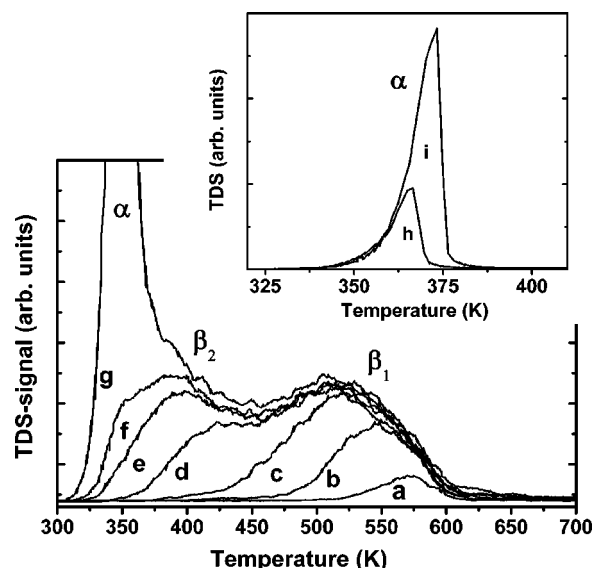


FIG. 2. Series of thermal desorption spectra (TDS) of 4P on Au(111) adsorbed at 93 K. The 4P coverage for each single TD spectrum is represented as mean 4P film thickness: (a) 0.02 nm, (b) 0.10 nm, (c) 0.15 nm, (d) 0.20 nm, (e) 0.25 nm, (f) 0.28 nm, and (g) 0.50 nm, respectively. The multilayer desorption feature is denoted by α and two distinct monolayer features are observed, β_1 and β_2 . The inset shows the thermal desorption of a (h) 2 nm and (i) a 7 nm thick 4P film in full scale. The zero-order characteristics of the multilayer desorption peak can be clearly seen.

exhibits the buildup of a peak around 550 K, labeled β_1 . With increasing coverage β_1 shifts to lower temperatures until it saturates at a mean total film thickness of about 0.15 nm. The mean film thickness was calculated from the adsorbed mass, as measured quantitatively with a quartz microbalance, using the 4P bulk density (1.25 g/cm³). At higher coverage a second peak, labeled β_2 , originates at about 400 K and roughly takes another 0.15 nm of mean 4P film thickness to saturate. The β_2 peak also shows a pronounced shift to lower temperatures with increasing coverage. This shift and the fact that the 4P adsorbs/desorbs as intact molecules on/from the Au(111) surface indicate a first-order desorption with repulsive forces acting within both the β_1 and β_2 adsorption states.¹⁹ The saturation coverage of the full 4P monolayer ($\beta_1 + \beta_2$) was quantified to 8×10^{13} molecules/cm², which equals a mean film thickness of about 0.3 nm. The determination of the desorption energy E_{des} and the preexponential factor²⁰ ν is a nontrivial task in the case of large aromatic molecules. Unusually large preexponential factors have been frequently observed in comparable systems.^{21,22} Things get even more complicated in case of desorption processes governed by lateral interactions between the adsorbate molecules (compensation effect).²³ Therefore, we abstained from a determination of these parameters for the β_1 and β_2 peaks. Considering the mean thickness of the 4P monolayer (0.3 nm) and taking into account the van der Waals dimensions of a single 4P molecule ($2.04 \times 0.67 \times 0.35$ nm³) it is reasonable to conclude that the 4P molecules are “lying” on the surface, i.e., the long molecular axes are oriented nearly parallel to the Au(111) surface.

At a 4P coverage > 1 ML, a sharp peak arises, labeled α ,

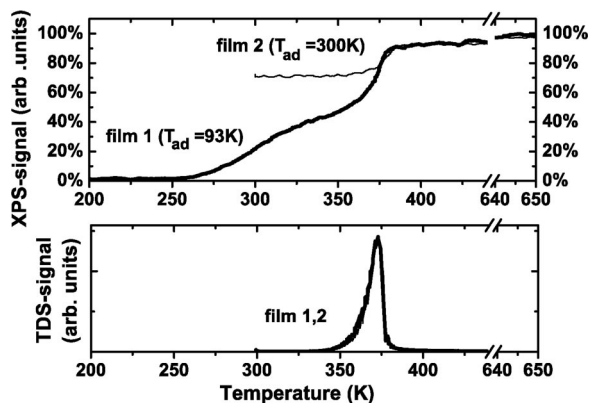


FIG. 3. Combined XPS and TDS measurement of 7 nm thick 4P films grown on Au(111) at different adsorption temperatures, T_{ad} , of 93 K and 300 K, respectively. The upper part shows the temperature dependence of the Au $4f_{7/2}$ signal, which is proportional to the fraction of uncovered Au(111) surface area. The lower part shows the TD spectra of equivalently deposited 4P films on the same substrate.

which increases continuously with increasing coverage, exhibiting a peak shift to higher temperature (see inset of Fig. 2). This peak can be attributed to zero-order desorption from the 4P multilayer. The desorption energy can easily be calculated in this case from the common leading edge, according to the Polanyi-Wigner formalism,²⁴ yielding $E_{des} = 1.52$ eV. This is in good agreement with the literature value for the 4P sublimation enthalpy of 1.62 eV.²⁵

B. Thin film growth and morphology

A combination of XPS and TDS, which will be denoted as “XPS vs Temp” measurements, has been applied to investigate the thin film growth kinetics and morphology of 4P on Au(111). The temperature dependence of the Au $4f_{7/2}$ signal of the underlying Au substrate was measured for a 7 nm thick 4P film deposited on Au(111). Details of this method are described in Ref. 16. In particular, it has been verified that the peak position of the Au $4f_{7/2}$ signal does not change with 4P coverage. Figure 3 shows XPS vs Temp (upper part) and the TDS (lower part) data of two 7 nm thick 4P films, deposited at different adsorption temperatures. To begin with the film adsorbed at 93 K (film 1), the XPS Au $4f_{7/2}$ signal is close to zero in a temperature range from 93 K up to 270 K. This is interpreted as being due to a continuous 4P film of unknown structure covering the whole Au(111) surface. In the temperature range from 270 to 310 K the XPS signal increases and runs into a flat “plateau” at about 350 K. In this range still no significant desorption occurs, as can be seen from the TDS underneath. Obviously, a recrystallisation of the 4P film takes place, where the formerly continuous film changes to a morphology of separated 4P islands. A further temperature increase leads to 4P multilayer desorption (325 K–375 K), where the Au $4f_{7/2}$ XPS signal also shows a sharp increase and then stagnates at about 90% of the signal of the clean Au(111) surface. At this point, only the 4P monolayer is still present on the surface. Finally, for temperatures >375 K the monolayer starts to desorb and correspondingly the XPS signal shows a slight increase until it reaches 100% at 650 K.

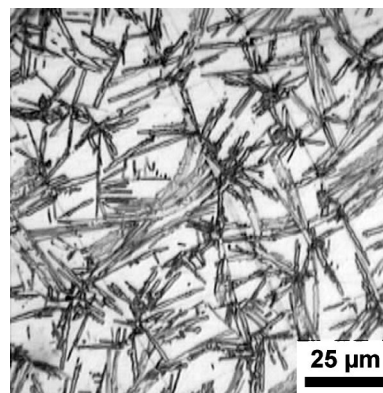


FIG. 4. Optical microscopy images of a 20 nm 4P film grown on Au(111) at 300 K and a deposition rate of 0.42 nm/min. Characteristic needle-shaped 4P islands are observed.

In contrast to that, a 7 nm thick 4P film adsorbed at 300 K (film 2) exhibits a significantly higher initial Au $4f_{7/2}$ signal. This elevated XPS signal of about 70% of the clean surface signal corresponds to an islandlike 4P layer. Apparently, the island height is on the average about 3.3 times higher than the mean film thickness at 93 K. The signal remains nearly constant until significant multilayer desorption sets in at about 350 K. A closer inspection shows that even at the beginning of multilayer desorption no significant change in the Au signal is observed. Obviously, the desorption process reduces mainly the height but not the lateral width of the 4P islands. Only when the last fraction of the multilayer desorbs (near 375 K), the XPS signal sharply increases. The mean height of the 4P islands at this point can be estimated from the mean free path, $\lambda = 2.4 \pm 0.3$ nm, of the Au $4f_{7/2}$ photoelectrons ($E = 1170$ eV) in 4P, as determined in a previous work.¹⁶ These findings suggest that 4P exhibits a layerlike growth at low temperatures and a Stranski-Krastanov (SK) growth at and above 270 K.

Figure 4 shows an OM image of a 20 nm thick 4P film grown on Au(111) at 300 K and at a deposition rate of 0.42 nm/min. Clearly, 4P forms needlelike islands of different lengths and orientations. However, the lateral needle width seems to be nearly constant throughout a single 4P needle. Several individual needles can agglomerate to form fanlike bunches. A maximum needle length of about 30 μm was observed and the width of the needles can be up to about 2.5 μm .

Whereas OM investigations provide a quick overview of the film morphology, AFM measurements allow a more detailed view with nanometer resolution in all three dimensions. Figure 5 summarizes the AFM results for the 200 nm thick 4P film grown at 300 K. This film shows four different morphological features with lateral extensions in the range of 10 μm that exist in close vicinity. The area denoted by *A* in Fig. 5(a) consists of parallel chains of tetragonal islands with a base edge length of about 1 μm . Their height is in the range of 200–250 nm. Within a single chain the islands are all identically oriented. This segmented structure of the 4P chains (“needles”) could not be resolved with OM. At least six different chain directions could be identified. Area *B* features significantly smaller, platelike crystallites. The struc-

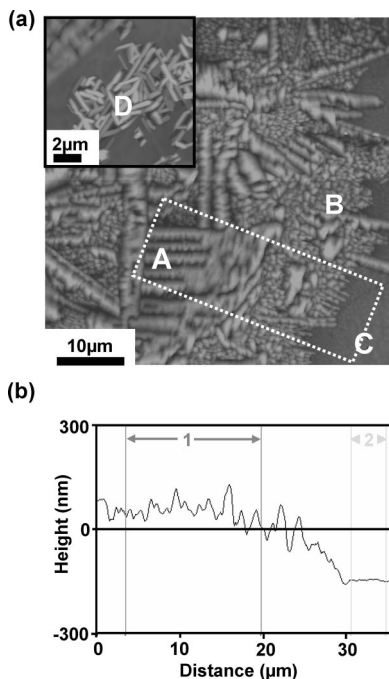


FIG. 5. High-resolution AFM results of the 200 nm 4P film grown at 300 K with a rate of ~ 0.4 nm/min. (a) $50 \times 50 \mu\text{m}^2$ AFM image (gray scale range is 600 nm). The inset shows a $10 \times 10 \mu\text{m}^2$ high resolution AFM image (gray scale range is 1 μm) of an additional structural feature. The dotted rectangle denotes the sample area used for the integral step height analysis presented in (b).

tural features *A* and *B* can either abut against each other or they can be separated by regions *C* free of three-dimensional islands. A fourth structural feature exists, which is presented with higher resolution in the inset of Fig. 5(a). This area *D* exhibits a loose group of individual crystallites with a length ranging from 0.8 μm to 2 μm . The cross-sectional analysis revealed that these islands are almost as high (250–550 nm) as wide (300–500 nm). In other words, these individual islands are rods with a nearly quadratic cross section. Figure 5(b) presents an integral step height analysis within the area marked by a dotted rectangle in Fig. 5(a). With this method the height signal is averaged across a line parallel to the short side of the marked area. This integral height is plotted against the lateral distance (long side of the marked area). The difference of the mean height is calculated between the intervals marked by 1 and 2, yielding a step height of about 200 nm between the uncovered area *C* and a fully covered part of the 4P film, which is in good agreement with the nominal film thickness previously measured with the quartz microbalance.

C. Epitaxially ordered bulk structure

Despite the inhomogeneous island morphology of thick 4P films, as shown in Figs. 4 and 5, the molecular arrangement within these islands was found to be highly regular with respect to the Au(111) surface. The 4P crystallites grow epitaxially on the Au(111) surface, as observed with XRD and LEED. Specular $\Theta/2\Theta$ scans of a 30 nm and a 200 nm thick 4P film shown in Fig. 6 revealed that the dominating crystalline orientation of the 4P bulk is one with the (211) net

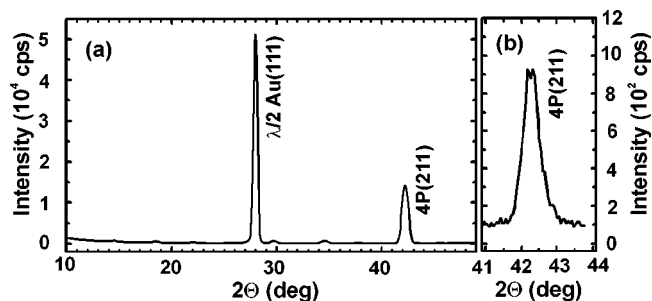


FIG. 6. (a) $\Theta/2\Theta$ scan between 10° and 50° of the 200 nm 4P film grown on Au(111) at 300 K. A single-crystal monochromator was used, therefore contributions of the x-ray spectrum can pass through the monochromator device at higher harmonics λ/n . (b) Detail $\Theta/2\Theta$ scan of the 4P(211) reflection recorded for the 30 nm 4P film grown on Au(111) at 320 K. Note the different ordinate scaling.

plane of 4P being parallel to the Au(111) substrate. It turns out that both the long axes and the short axes of the 4P molecules are lying parallel to the (211) plane. In addition, previous measurements using the x-ray diffraction pole figure technique have shown the influence of the Au(111) substrate geometry on the azimuthal ordering of the 4P overlayer. The long axes of the 4P molecules are azimuthally aligned along high-symmetry directions of the Au substrate, i.e., the Au $\langle 1\bar{1}0 \rangle$ or the Au $\langle 11\bar{2} \rangle$ directions, respectively. Details are described in Ref. 26.

D. Surface structure

1. Monolayer

Some results of the 4P monolayer on Au(111) have been published previously in Ref. 26. In the present study, these results are briefly summarized for the sake of completeness, and some additional aspects will be discussed. The highly regular 4P monolayer grown on Au(111) exhibits an oblique unit cell with side lengths $a = 1.1$ nm and $b = 2.2$ nm, comprising two molecules in the unit cell. The cell angle is $\gamma = 74^\circ$.²⁶ The 4P molecules are aligned with their long axes either parallel to the Au $\langle 1\bar{1}0 \rangle$ or to the Au $\langle 11\bar{2} \rangle$ direction, analogous to the alignment of the molecules in the (211) plane of the bulk structure with respect to the Au(111) surface.

It is well-known that the Au(111) surface reconstructs with a $(23 \times \sqrt{3})$ surface unit cell,^{27,28} causing additional LEED reflections with respect to an ideal fcc(111) surface.²⁹ After the deposition of 1 ML 4P these extra spots vanish. Although it could not be unambiguously clarified if the Au reconstruction is lifted by the presence of a 4P overlayer, there is evidence that the growth of a regular 4P structure is nearly independent of a possible reconstruction. The LEED images of the 4P superstructure on Au(111) exhibited the same spots as expected for 4P grown on an ideal fcc(111) surface. This suggests that a possible Au surface reconstruction has no significant influence on the formation of a regular 4P superstructure, concerning the size and orientation of the 4P surface unit cell relative to the Au(111) surface. The lateral and vertical displacements of the reconstructed gold sur-

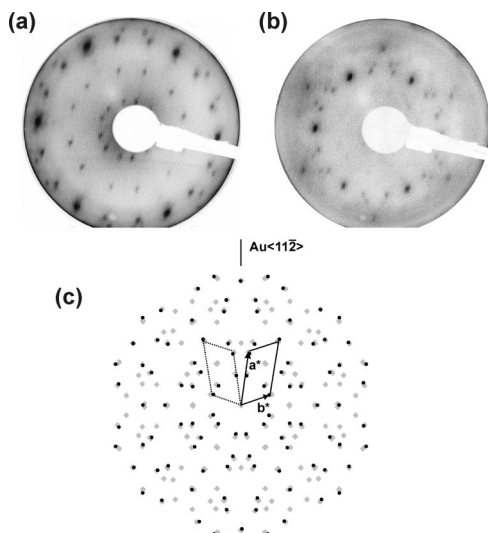


FIG. 7. LEED images of a 0.5 ML 4P films grown on Au(111). The corresponding beam voltages are (a) 19.8 V and (b) 39.4 V, respectively. (c) Representation of the LEED pattern free of image deformations. The black circle symbols (●) correspond to experimentally observed spots and the light diamond symbols (◇) represent the simulated reflections. The reciprocal unit cell vectors are denoted by a^* and b^* . Additionally, an example of a mirrored unit cell is shown (dotted).

face are just too small to influence the orientation of the large 4P molecules. This is similar to previous findings for SubPc grown on Au(111).³⁰

At substrate temperatures below 270 K no regular LEED pattern could be observed for the 4P monolayer on Au(111). However, for adsorption at room temperature, or when heating the covered sample from 93 K up to 270 K a regular LEED pattern is formed. These findings corroborate the previously observed onset of recrystallization of thick 4P films at about the same temperature. The 4P monolayer LEED pattern did not change upon further heating of the sample until 4P desorption starts. Different from that, recent findings for 6P on Al(111) showed the existence of different, temperature-dependent monolayer structures.³¹

2. Submonolayer

Well ordered and highly reproducible LEED patterns have also been observed for a 4P coverage of 0.5 ML on Au(111) (saturation of the β_1 peak). A series of LEED images was taken for beam voltages between 17 V and 40 V. Figures 7(a) and 7(b) show examples of the 0.5 ML 4P LEED pattern at a voltage of 19.8 V and 39.4 V, respectively. After extracting the positions of all visible spots from a series of LEED images (the intensity of individual spots varied considerably with beam voltage) and correcting for image deformations of the LEED optics, a representation of the 0.5 ML 4P LEED pattern is obtained [black dots in Fig. 7(c)]. A reciprocal surface unit cell is proposed, also shown in Fig. 7(c), which can explain all the observed spots. However, taking into account the threefold rotational symmetry of the (111) surface and the possibility of mirrored structures for each rotational domain, additional spots should show up. All possible spots in connection with the proposed reciprocal unit cell are represented as grey diamonds in Fig. 7(c). Ap-

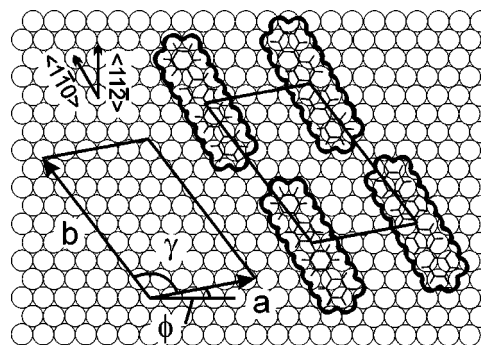


FIG. 8. Real space representation of the 0.5 ML 4P surface unit cell on Au(111). The side lengths of the cell, the cell angle, and the azimuthal rotation angle relative to the Au(111) surface are denoted by a , b , γ , and Φ , respectively. A proposed van der Waals model of azimuthally oriented 4P molecules is shown on the right part.

parently, due to the (unknown) geometrical structure factor of the 4P unit cell some of the possible reflections are suppressed. The dimensions of the real space surface unit cell are represented in Fig. 8. In absolute values they read as $a = 1.44$ nm, $b = 2.38$ nm, $\gamma = 117^\circ$, and $\Phi = 10.5^\circ$, respectively. The matrix notation for this superstructure is

$$M = \begin{pmatrix} 5.44 & 1.05 \\ -1.25 & 7.57 \end{pmatrix} \approx \begin{pmatrix} 5.5 & 1 \\ -1.25 & 7.5 \end{pmatrix}. \quad (1)$$

The characteristic length of the b side, which is about equal to the van der Waals length of a 4P molecule, suggests a molecular packing, where the long axes of the 4P molecules are aligned roughly parallel to the b side. Based on the results of the monolayer structure we also propose for the 0.5 ML structure an alignment of the 4P molecules parallel to the $\langle 1\bar{1}0 \rangle$ direction of the Au(111) surface. The area of the real space surface unit cell is about 2.9 nm². Given a basis of one 4P molecule per unit cell, the 0.5 ML film corresponds to a 4P coverage of about 3.3×10^{13} molecules/cm² or 0.13 nm of mean film thickness. This is in good agreement with the TDS experiments, where a saturation coverage of about 0.15 nm was observed for the high-temperature adsorption state, β_1 .

Compared to the full 4P monolayer structure, the length of the short cell vector, a , of the 0.5 ML structure is increased by about 30%, whereas the length of the long cell vector, b , is hardly changed. Assuming flat lying molecules within the 0.5 ML structure, as indicated by TDS and XRD,²⁶ a molecular packing is obtained with a surprisingly large intermolecular spacing in the direction of a as shown in Fig. 8. This enlargement can be interpreted as a result of repulsive forces acting between neighboring molecules over distances up to about 0.6 nm. The repulsive character of the interaction is affirmed by the TDS data. The large distance of about 0.6 nm suggests the existence of long-range interactions different from the intermolecular van der Waals-type interactions. Presumably, 4P molecules adsorbed on the Au(111) induce localized surface dipole densities due to the interaction with the metallic substrate, resulting in a long-range repulsion between neighboring adsorbate molecules. Actually, similarly large intermolecular spacings in the submonolayer coverage regime have recently been observed for

perylene on Au(110) (Ref. 32) or Pentacene on Au(111).³³ Apparently, in the full 4P monolayer the presence of the β_2 -type adsorbed molecules (i.e., the side-tilted molecules²⁶) decreases the long-range repulsion between neighboring β_1 -type molecules. This is a consequence of the herringbone-like packing of the 4P molecules which is already established in the first saturated 4P monolayer. An optimized herringbone packing is finally reached in the 4P bulk phase of thicker films.²⁶

IV. SUMMARY

Adsorption, thin film growth, and film structure of 4P on Au(111) was investigated over a wide coverage range. Thermal desorption spectroscopy revealed the existence of two adsorption states in the monolayer regime, which are clearly separated from the multilayer state. The shape of the monolayer spectrum indicates repulsive forces acting within the monolayer. Quantitative TDS yields a saturation coverage of 8×10^{13} molecules/cm² or 0.3 nm of mean film thickness for the 4P monolayer. Combined XPS and TDS studies show that at 93 K both the monolayer and the multilayer grow in form of a disordered layerlike structure. During sample heating the disordered layer recrystallizes at about 270 K to highly ordered, needle-shaped islands, on top of an ordered monolayer (wetting layer). Adsorption at room temperature also leads to a Stranski-Krastanov-like growth mode, but with different island morphologies, as observed with combined XPS-TDS. The monolayer structure, as investigated by LEED, can be described by an oblique surface unit cell containing two molecules in the basis, one flat lying and one side-tilted molecule, with the long axes of the molecules being parallel to the $\langle 1\bar{1}0 \rangle$ rows of the Au(111) surface. At half-monolayer coverage a different structure was observed, with an expanded surface unit cell and only one molecule in the basis. The relatively large intermolecular distance is most probably due to repulsive forces acting between neighboring 4P molecules adsorbed on the Au(111) surface, consistent with the TDS results. The determination of the crystal bulk structure of the 4P islands by x-ray diffraction revealed the epitaxial growth of quaterphenyl. The dominant crystal orientation is the 4P(211) plane parallel to the Au(111) plane. The long axes of the 4P molecules are azimuthally locked to high symmetry directions of the Au(111) surface. This demonstrates that the monolayer is a prestage of the epitaxial multilayer growth.

ACKNOWLEDGMENTS

This work was supported by the Austrian "Fonds zur Förderung der wissenschaftliche Forschung," Project Nos.

P15625 and P15626. We kindly appreciate the experimental support of T. Haber for the XRD-PF measurements and S. Holzleitner for technical assistance in the AFM measurements.

- ¹ S. R. Forrest, *Chem. Rev.* (Washington, D.C.) **97**, 1793 (1997).
- ² J. Kalinowski, *J. Phys. D* **32**, R179 (1999).
- ³ C. D. Dimitrakopoulos and D. J. Mascaró, *IBM J. Res. Dev.* **45**, 11 (2001).
- ⁴ S. Tasch, C. Brandstaetter, F. Meghdadi, G. Leising, G. Froyer, and L. Athouel, *Adv. Mater. (Weinheim, Ger.)* **9**, 33 (1997).
- ⁵ M. Era, T. Tsutsui, and S. Saito, *Appl. Phys. Lett.* **67**, 2436 (1995).
- ⁶ D. J. Gundlach, Y. Y. Lin, T. N. Jackson, and D. G. Schlom, *Appl. Phys. Lett.* **71**, 3853 (1997).
- ⁷ E. Umbach, K. Glöckler, and M. Sokolowski, *Surf. Sci.* **402–404**, 20 (1998).
- ⁸ F. Rosei, M. Schunack, Y. Naitoh *et al.*, *Prog. Surf. Sci.* **71**, 95 (2003).
- ⁹ L. Athouel, G. Froyer, M. T. Riou, and M. Schott, *Thin Solid Films* **274**, 35 (1996).
- ¹⁰ R. Resel, *Thin Solid Films* **433**, 1 (2003).
- ¹¹ A. Andreev, G. Matt, C. J. Brabec, H. Sitter, D. Badt, H. Seyringer, and N. S. Sariciftci, *Adv. Mater. (Weinheim, Ger.)* **12**, 629 (2000).
- ¹² E. Zojer, N. Koch, P. Puschnig *et al.*, *Phys. Rev. B* **61**, 16538 (2000).
- ¹³ F. Balzer, V. G. Bordo, A. C. Simonsen, and H.-G. Rubahn, *Phys. Rev. B* **67**, 115408 (2003).
- ¹⁴ P. Puschnig and C. Ambrosch-Draxl, *Phys. Rev. B* **60**, 7891 (1999).
- ¹⁵ S. Müllegger and A. Winkler, *Surf. Sci.* (to be published).
- ¹⁶ S. Müllegger, O. Stranik, E. Zojer, and A. Winkler, *Appl. Surf. Sci.* **221**, 184 (2004).
- ¹⁷ Y. Delugeard, J. Desuche, and J. L. Baudour, *Acta Crystallogr., Sect. B: Struct. Crystallogr. Cryst. Chem.* **B32**, 702 (1976).
- ¹⁸ K. N. Baker, A. V. Fratini, T. Resch, H. C. Knachel, W. W. Adams, E. P. Socci, and B. L. Farmer, *Polymer* **34**, 1571 (1993).
- ¹⁹ R. I. Masel, *Principles of Adsorption and Reaction on Solid Surfaces* (Wiley, New York, 1996).
- ²⁰ D. A. King, *Surf. Sci.* **47**, 384 (1975).
- ²¹ S. Yu. Krylov and L. J. F. Hermans, *Phys. Rev. B* **65**, 092205 (2002).
- ²² K. R. Paserba and A. J. Gellman, *Phys. Rev. Lett.* **86**, 4338 (2001).
- ²³ D. L. S. Nieskens, A. P. van Bavel, and J. W. Niemantsverdriet, *Surf. Sci.* **546**, 159 (2003).
- ²⁴ P. A. Redhead, *Vacuum* **12**, 203 (1962).
- ²⁵ A. A. Balepin, V. P. Lebedev, E. A. Miroshnichenko, G. I. Koldobskii, V. A. Ostovskii, B. P. Larionov, B. V. Gidasov, and Yu. A. Lebedev, *Svoistva Veshchestv Str. Mol.* **93–98**, (1977).
- ²⁶ S. Müllegger, I. Salzmann, R. Resel, and A. Winkler, *Appl. Phys. Lett.* **83**, 4536 (2003).
- ²⁷ Ch. Wöll, S. Chiang, R. J. Wilson, and P. H. Lippel, *Phys. Rev. B* **39**, 7988 (1989).
- ²⁸ J. V. Barth, H. Brune, G. Ertl, and R. J. Behm, *Phys. Rev. B* **42**, 9307 (1990).
- ²⁹ M. A. Van Hove, R. J. Koestner, P. C. Stair, J. P. Bibérian, L. L. Kesmodel, I. Bartos, and G. A. Somorjai, *Surf. Sci.* **103**, 189 (1981).
- ³⁰ S. Mannsfeld, H. Reinhard, and T. Fritz, *Surf. Sci.* **525**, 215 (2003).
- ³¹ B. Winter, J. Ivanco, F. P. Netzer, and M. G. Ramsey, *Thin Solid Films* **433**, 269 (2003).
- ³² C. Seidel, R. Ellerbrake, L. Gross, and H. Fuchs, *Phys. Rev. B* **64**, 195418 (2001).
- ³³ C. B. France, P. G. Schroeder, J. C. Forsythe, and B. A. Parkinson, *Langmuir* **19**, 1274 (2003).